small NANO MICRO

Photodetectors

Synergetically Enhanced Near-Infrared Photoresponse of Reduced Graphene Oxide by Upconversion and Gold Plasmon

*Wenbin Niu, Hu Chen, Rui Chen, Jingfeng Huang, Alagappan Palaniappan, Handong Sun, Bo Gunnar Liedberg, and Alfred Iing Yoong Tok**

Near-infrared photodetectors have found many uses in electronic devices ranging from image sensor array,[1a,b] remote control devices,[1c,d] to multiplexed bio-sensor array.[1e] Graphene, as material for future electronic and optoelectronic applications, has attracted tremendous research interests due to its unique optical and electronic properties.[2] In particular, the wideband absorption, high room-temperature carrier mobility, and short carrier lifetime make graphene the ideal material for wideband and high-speed photodetectors.[1d,3] Recent studies have demonstrated the exciting potential of exploiting graphene as ultrafast infrared photodetectors for high-speed optical communications.[1d,4] However, the performance of graphene-based near-infrared photodetectors is limited by its low photoresponsivity due to the low light absorption (≈2% of normal incident light).[2,4,5] To improve near-infrared responsivity, graphene film was modified with quantum dots (e.g., PbS) that can absorb near-infrared light more efficiently, from which the photogenerated charges transfer to graphene, thus improving carrier mobility and the photoresponse of devices.[5b,6] However, those colloidal quantum dots still suffer from their intrinsic drawbacks such as high toxicity, and low photo- and chemical-stability.[7] It is therefore necessary to develop a new route for enhancing responsivity of the near-infrared photodetectors.

Lanthanide-doped upconversion nanoparticles (UCNPs), which are capable of converting near-infrared radiation into shorter wavelength through an upconversion process, exhibit low toxicity, superior photo- and chemical-stability,[8,9] giving potential applications in remote control devices,[10] drug delivery,[11] and solar cell, and so forth.[12] Among various upconversion materials, lanthanide-ion doped $NaYF_4$ has been shown to be the most efficient UCNPs, because the low phonon energy of $NaYF_4$ host suppresses nonradiative multiphonon relaxation processes of activators.[12,13] As a typical example, $NaYF_4$:Yb,Tm UCNPs can convert near-infrared excitation light into characteristic UV and blue emissions, which can readily be absorbed by graphene as the absorbance of graphene sharply increased from infrared to UV region.[2b-d] Therefore, this paper hypothesize that combining $NaYF_4$:Yb,Tm UCNPs with graphene will improve the responsivity of near-infrared photodetectors by upconverting near-infrared light into short wavelength emissions.

It is known that placing UCNPs in close proximity to plasmonic metal nanostructure surfaces such as Au and Ag nanoparticles could enhance their upconversion emissions, because metal nanostructures could create a surface-bound electric field which can increase excitation rates and radiative decay rates of UCNPs.[14] Many researchers have reported the enhancement of upconversion emissions from several to several dozen times based on Au and Ag plasmon.[14,15] For example, Saboktakin et al. demonstrated gold plasmonic-enhanced upconversion emissions of $NaYF_4$:Yb/Er nanoparticles with a factor of 5.[15a] On the other hand, it is reported that metal plasmonic nanostructures-created local electric field near graphene could enhance the overall absorption of graphene, resulting in the improvement of photoresponsivity.[16] If UCNPs-graphene nanocomposites were further coupled with metal plasmonic nanoparticles, the responsivity might be further improved for a UCNPs-metal nanoparticles-based graphene near-infrared photodetector. Herein, in this study, we present a new route to fabricating highly sensitive near-infrared photodetectors by integrating graphene with UCNPs and a thin layer of plasmonic nanostructures.

Chemical reduction of graphene oxide (GO) offers an effective route of graphene synthesis,[2] allowing graphene-based devices to be fabricated in a low-cost, large-scale and facile manner.[2] Thus, reduced graphene oxide (rGO) was used for the preparation of graphene-based devices in this study. Hexagonal phase $NaYF_4$:Yb,Tm@$NaYF_4$ core/shell UCNPs (Figure S1, Supporting Information), synthesized according to a modified thermolysis method in the presence of oleic acid and octadecene,[8] were selected for the enhancement of rGO-based photodetectors because of its

Dr. W. B. Niu, H. Chen, J. Huang, Prof. A. I. Y. Tok
School of Materials Science and Engineering
Nanyang Technological University
50 Nanyang Avenue, 639798, Singapore
E-mail: MIYTok@ntu.edu.sg
Dr. R. Chen, Prof. H. D. Sun
School of Physical and Mathematical Sciences
Nanyang Technological University
50 Nanyang Avenue, 639798, Singapore
Dr. A. Palaniappan, Prof. B. G. Liedberg
Center of Biom Sensor Science
Nanyang Technological University
50 Nanyang Avenue, 639798, Singapore

DOI: 10.1002/smll.201400400

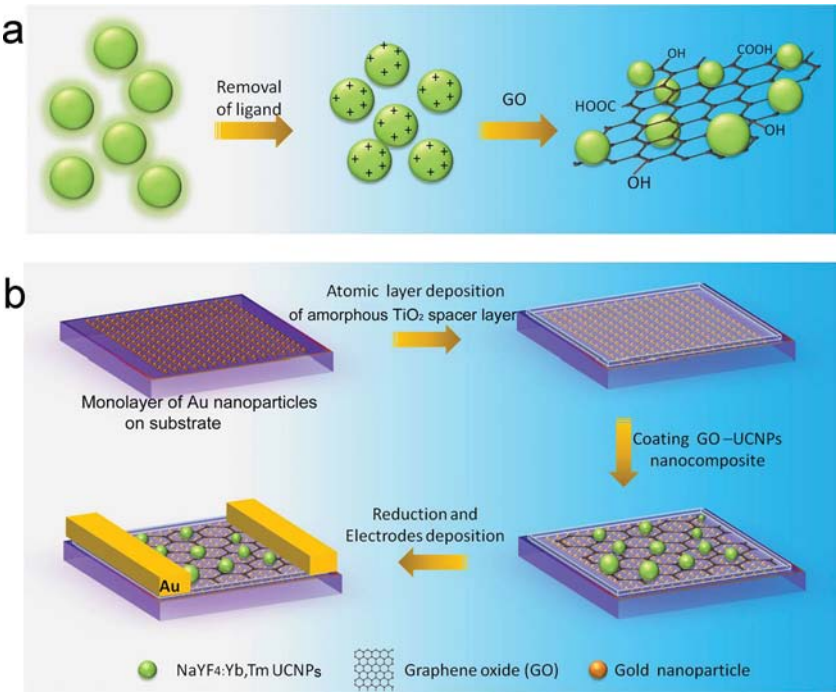

Scheme 1. Schematic illustration of the fabrication processes of a) GO- $NaYF_4$:Yb,Tm@$NaYF_4$ UCNPs nanocomposites and b) upconversion and plasmon-coupled graphene devices with the structure of Au nanoparticles–amorphous TiO_2 layer–UCNPs rGO nanocomposites.

strong UV and blue emissions.[9] **Scheme 1** shows experiment procedure for the fabrication of near-infrared photoresponse devices. This consists of two main procedures: 1) preparation of GO-$NaYF_4$:Yb,Tm@$NaYF_4$ UCNPs nanocomposites (Scheme 1a), and 2) fabrication of UCNPs and gold plasmon enhanced near-infrared photoresponse devices (Scheme 1b). In the present work, GO-UCNPs nanocomposites were prepared via coordination interaction. To obtain ligand-free UCNPs for the formation of GO-UCNPs nanocomposites, the prepared oleate-capped $NaYF_4$:Yb,Tm@$NaYF_4$ core/shell nanoparticles were treated with 0.1 m HCl aqueous solution,[8a,17] which protonated oleate ligands resulting in the release of oleic acid from particle surface and the formation of positively charged ligand-free UCNPs in aqueous solution.[8a,17] The measured zeta potential of +35 mV at pH 3 suggests that UCNPs are colloidal stable and dispersed by electrostatic stabilization forces, as a large zeta potential usually ±25 mV indicates a stable colloidal system that is the absence of coagulation.[17] Generally, GO has abundant carboxyl and hydroxyl groups that can easily interact with metal ions.[13a,b] After addition of as-prepared UCNPs with positively-charged surface, GO easily interacted with metal ions on the surface of UCNPs at low pH conditions to form GO-UCNPs nanocomposites. The corresponding transmission electron microscopy (TEM) images of $NaYF_4$:Yb,Tm@$NaYF_4$ UCNPs and GO employed to prepare nanocomposites were shown in **Figure 1**a and 1b, respectively. Figure 1c and 1d show TEM images of the obtained GO-$NaYF_4$:Yb,Tm@$NaYF_4$ UCNPs nanocomposites. It is shown that UCNPs with size of around 50 nm were anchored on GO sheet, and even a small amount of them were encapsulated by GO sheet, indicating the formation of GO-$NaYF_4$:Yb,Tm@ $NaYF_4$ UCNPs nanocomposites.

FT-IR spectra provide more details on the interaction between UCNPs and GO sheet in their nanocomposites (**Figure 2**). Oleate-capped UCNPs usually exhibited the strong characteristic absorption bands of oleate ligand (Figure 2a): the asymmetric and symmetric stretching vibrations of methylene (CH_2 at 2924 and 2853 cm^{-1}) and carboxyl groups (COO-, at around 1465 and 1564 cm^{-1}),[18] which clearly demonstrated the chemical adsorption of oleic acid molecules on UCNPs surface through coordination interaction between COO- group and rare earth ions, in comparison with those of oleic acid molecules (Figure S2, Supporting Information).[17] After treatment in HCl solution, there is no characteristic stretchings of methylene and carboxylate, indicating the removal of oleate ligand from UCNPs surface due to protonation process (Figure 2b).[17] For GO generated by oxidation (Figure 1c), there were characteristic bands at 1719 and 1631 cm^{-1} attributed to the vibrations of C = O in carboxyl group and C = C in aromatic system,[13a,19] and the peaks at 1224 and 1048 cm^{-1} attributed to aether (C–O–C) and C–OH stretching vibrations,[19,20] respectively. In addition, the methylene stretchings of CH_2 moiety in GO was also shown at 2924 and 2853 cm^{-1}. For GO-UCNPs nanocomposites in Figure 1d, the peak at 1719 cm^{-1} was greatly weakened, implying the coordination interaction between carboxyl group and rare earth ions on oleate-free UCNPs.[13a,21] The absence of the peaks at 1224 and 1576 cm^{-1} and the appearance of the peak at 1104 cm^{-1} further suggest the chemical interactions between fluoride UCNPs and GO.[13a]

To improve the near-infrared photoresponsivity of rGO-based devices, a monolayer layer of gold nanoparticles was further coupled to nanocomposites (Scheme 1b).[14a,15a] Specifically, a 4 nm gold film was first sputtered on substrate, followed by a thermal annealing at 350 °C for 15 min to form a high density monolayer of gold nanoparticles with an average diameter ≈28 nm as shown in **Figure 3**a. To maximize the upconversion enhancement, a layer of amorphous TiO_2 with 8 nm thickness was grown onto the surface of gold nanoparticles layer by atomic layer deposition (ALD) method (Scheme 1b), because the close proximity to the surface of gold nanostructures would result in the quenching of luminescence due to resonant energy transfer.[14a,15] The deposited TiO_2 layer induced a slightly red shift of plasmonic peak of gold nanoparticles from 545 to 600 nm (Figure 2b), indicating that the amorphous oxide layer also plays an active role in the enhancement of plasmonic field by affecting the polarization of gold nanostructures.[22] Similar result was also observed in the ≈68 nm gold nanoparticles layer prepared by 8 nm thick gold film (Figure S4, Supporting Information). Next a layer of GO-UCNPs nanocomposites was drop-casted

small 2014,
DOI: 10.1002/smll.201400400

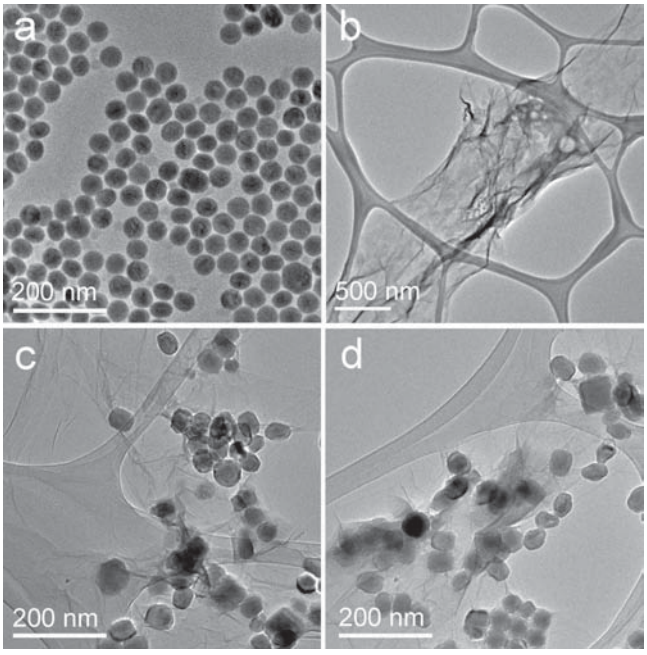

Figure 1. TEM images of a) $NaYF_4$:Yb,Tm@$NaYF_4$ UCNPs, b) GO nanosheet, and c,d) GO-$NaYF_4$:Yb,Tm@$NaYF_4$ nanocomposites.

on the top of the oxide layer and reduced to form rGO-UCNPs nanocomposites for devices fabrication (Scheme 1b).

The corresponding upconversion emission spectra were collected and shown in Figure 3c. We can clearly observe the characteristic emission bands of Tm^{3+} ion centered at 363 nm in the UV resulting from $^1D_2 \rightarrow {}^3H_6$ transition, at 450 and 477 nm in the blue resulting from $^1D_2 \rightarrow {}^3F_4$ and $^1G_4 \rightarrow {}^3H_6$ transitions, and at 800 nm ascribed to $^3H_4 \rightarrow {}^3H_6$ transition.[8b,13g,14b,23] In comparison with ligand-free $NaYF_4$:Yb,Tm@$NaYF_4$ core/shell UCNPs, the combination of GO and subsequent reduction decreased upconversion emission intensities (Figure 3c), which indicates the upconversion luminescence from $NaYF_4$:Yb,Tm@$NaYF_4$ nanoparticles was partially quenched by rGO. Further coupling rGO-UCNPs nanocomposites with 28 nm gold nanoparticles with an ALD deposited TiO_2 spacer layer leads to ≈1.5-fold

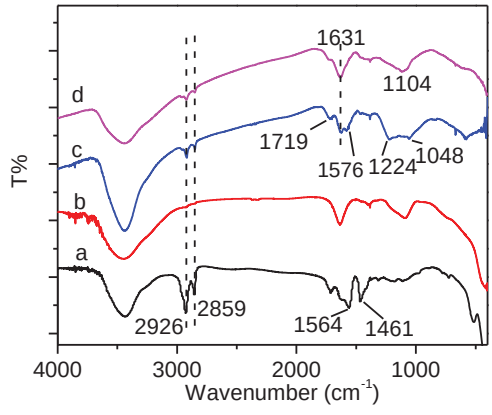

Figure 2. FT-IR spectra of a) oleate-capped and b) ligand-free $NaYF_4$:Yb,Tm@$NaYF_4$ UCNPs, c) GO nanosheet, and d) GO-$NaYF_4$:Yb,Tm@$NaYF_4$ nanocomposites.

enhancement of upconversion emissions, evidenced the plasmonic enhancement effect. Due to the increased local optical field with increasing gold nanoparticle size, upconversion emissions can be further increased by increasing the gold nanoparticle size to 68 nm (obtained by annealing 8 nm thick gold film, Figure S5, Supporting Information).[16a]

To probe the variation mechanism of upconversion emissions, the corresponding time-resolved upconversion spectra of 363 nm emission of Tm^{3+} ion were measured. The rise and decay curves were fitted by exponential function. Results show that the lifetimes of UCNPs decreased from 614 μs in ligand-free $NaYF_4$:Yb,Tm@$NaYF_4$ UCNPs to 540 μs in rGO-UCNPs nanocomposites. Such a reduced lifetime indicates the existence of fluorescence resonance energy transfer (FRET) in rGO-UCNPs nanocomposites, that is, the upconverted energy could be transferred from excited energy levels of Tm^{3+} ion to rGO via FRET mechanism,[8e,13c,e] thus resulting in the decrease of upconversion emission. This is reasonable because the strong absorption region of rGO at short wavelength matches well with the upconversion emissions of Tm^{3+} ion at around 363 and 477 nm (**Figure 4**a and Supporting Information Figure S3). In addition, it is reported that Förster radius was around 1.5 nm for UCNPs with colloidal CdSe QDs due to low quantum yield of the multilevel emitting of UCNPs.[8e-h,9c], In our system, these results further indicate that UCNPs closely contacted to rGO, and imply that UCNPs are anchored on GO before hydrazine reduction. After coupling with gold nanoparticles layer, the lifetimes further reduced to 521 μs, suggesting gold nanoparticles-induced Purcell effect due to the electromagnetic coupling increased the radiative rates, thereby enhancing upconversion emissions.[14a,15a] Apart from the plasmon-enhanced radiative decay rates, measurements revealed that gold plasmon also induced the decreasing of rise time from 257 to 196 μs. This indicates the non-resonant enhancement of excitation pump at 980 nm by gold nanoparticles enhanced the absorption process in Yb^{3+} ion, and thereby increased the rate of energy transfer from Yb^{3+} to Tm^{3+} ions.[14,15] As a result, the higher upconversion emissions were observed. That is, the gold plasmon-induced absorption enhancement and emission enhancement both contribute to the upconversion amplification of rGO-UCNPs nanocomposites. In addition, it is observed that upconversion emission of rGO-UCNPs composites on TiO_2 spacer layer-covered gold nanoparticles was higher than that of rGO-UCNPs composites alone, but lower than that of UCNPs with gold nanoparticles and the spacer layer (Figure S6, Supporting Information). Therefore, from the above discussion, it is concluded that the FRET procedure from UCNPs to rGO was responsible for the reduction of upconversion emissions in rGO-UCNPs nanocomposites with respect to ligand-free UCNPs. Further coupling rGO-UCNPs nanocomposites with gold nanoparticles layer with a spacer enhanced the upconversion intensities by ≈1.5 times due to both plasmonic enhancement of the emission of the UCNPs and metal-induced enhancement of absorption of the excitation pump at 980 nm.

As proof-of-concept experiments, photoresponse devices with the corresponding materials were fabricated to investigate their photoresponsivity upon 980 nm near-infrared light

DOI: 10.1002/smll.201400400

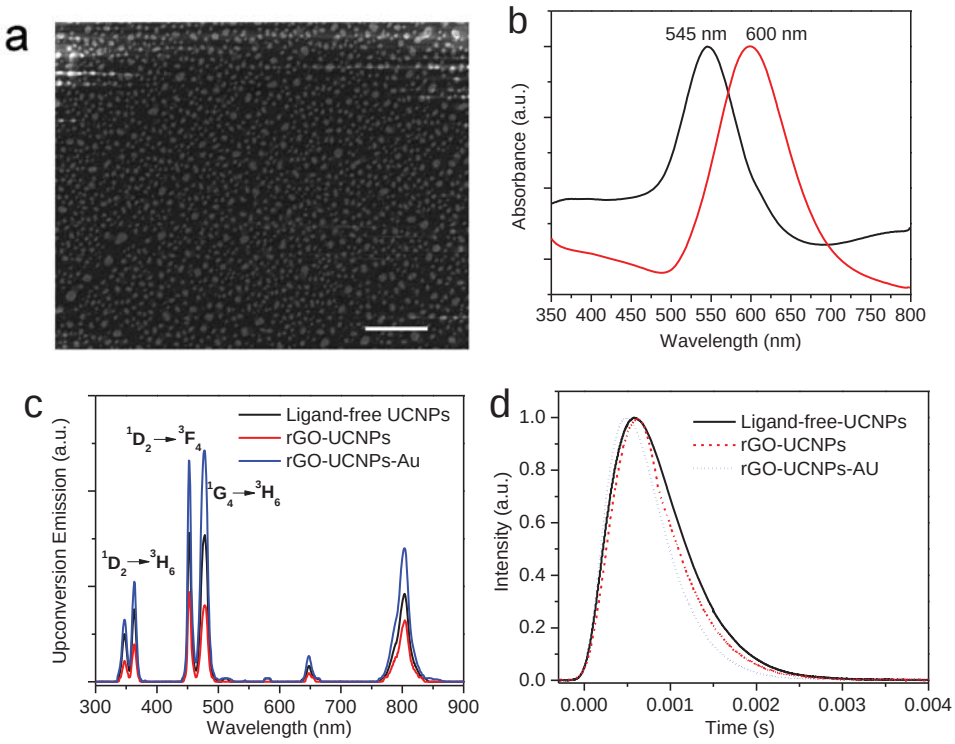

Figure 3. a) Field emission scanning electron microscopy (FESEM) image of the obtained gold nanoparticles on substrate by annealing a 4 nm thick gold thin film, scale bar 500 nm. b) absorption spectra (normalized) of the monolayer gold nanoparticles before (black curve) and after (red curve) deposition of an amorphous oxide spacer layer, c) upconversion luminescence spectra and d) lifetimes of 363 nm emission of Tm^{3+} ion under 980 nm excitation of $NaYF_4$:Yb,Tm@$NaYF_4$ UCNPs, rGO-$NaYF_4$:Yb,Tm@$NaYF_4$ UCNPs nanocomposites and rGO-$NaYF_4$:Yb,Tm@$NaYF_4$ UCNPs nanocomposites on the oxide layer-covered gold nanoparticles film.

irradiation. Figure 4b shows the normalized drain current of the photoresponse devices as a function of time for a representative four cycles. Here, a source-drain voltage (V_{DS}) of 10 mV was applied in the absence of gate bias. Control device prepared with rGO alone showed a very low drain current change (around 0.5%) because of the weak absorption of rGO to 980 nm near-infrared excitation (Figure 4a). The introduction of $NaYF_4$:Yb,Tm@$NaYF_4$ UCNPs improved photocurrent by more than 3.5 times. This implies that UCNPs are responsible for the increased near-infrared photoresponse behavior, because the upconverted photons can be readily absorbed by rGO through FRET procedure for charge separation as aforementioned. After further coupling with 28 nm gold nanoparticles layer with oxide spacer, the average photocurrent of the device exceeded those obtained on rGO alone and rGO-UCNPs nanocomposites by more than 7 and 2 times, respectively (Figure 4b). Importantly, it is noted that the coupling of rGO-UCNPs nanocomposites with 68 nm-diameter gold nanoparticle layer can achieve a photocurrent enhancement by more than 10 times with respect to the control device with rGO alone (Figure S7, Supporting Information). These experiment results agree well with the trend of upconversion emission spectra (Figure 3c and Supporting Information Figure S5), in which the upconversion enhancement increases with increasing gold nanoparticles size. This indicates that the rGO is able to absorb the gold plasmon-enhanced upconversion emissions, thus further improving the photoresponsivity to 980 nm near-infrared light. In addition to the plasmon-enhanced upconversion emissions, plasmon resonance-enhanced absorption of graphene in devices has also been reported to play an important role in photoresponsivity enhancement,[16a] which could contribute to the observed enhancement in our devices as well (Figure S8, Supporting Information).[16a] That is also why the upconversion enhancement factor was lower than those observed in other reports.[14,15] Nonetheless, regardless of the exact mechanism for photoresponsivity enhancement by gold plasmon, the coupling of both UCNPs and gold nanoparticles amplified the overall photoresponsivity of rGO-based photodetectors to near-infrared light.

In summary, we have demonstrated a new route to improving responsivity of rGO-based near-infrared photodetectors by coupling upconversion and gold plasmon. In the device fabricated with rGO-UCNPs nanocomposites, rGO absorbed upconverted shorter wavelengths light via FRET procedure, improving the photoresponsivity to 980 nm near-infrared light by more than 3 times with respect to the control device with rGO alone. Further coupling rGO-UCNPs nanocomposites with thin plasmonic layer enhanced upconversion intensities by increasing the radiative rate of emissions and the absorption of Yb^{3+} ion of UCNPs, which together with plasma-enhanced rGO absorption resulted in an overall enhancement of photoresponsvity by a factor of ≈10. This is the first demonstration of the application of coupling rGO with both upconverter and metal plasmon in enhancing photoresponsivity of near-infrared photodetectors,

small 2014,
DOI: 10.1002/smll.201400400

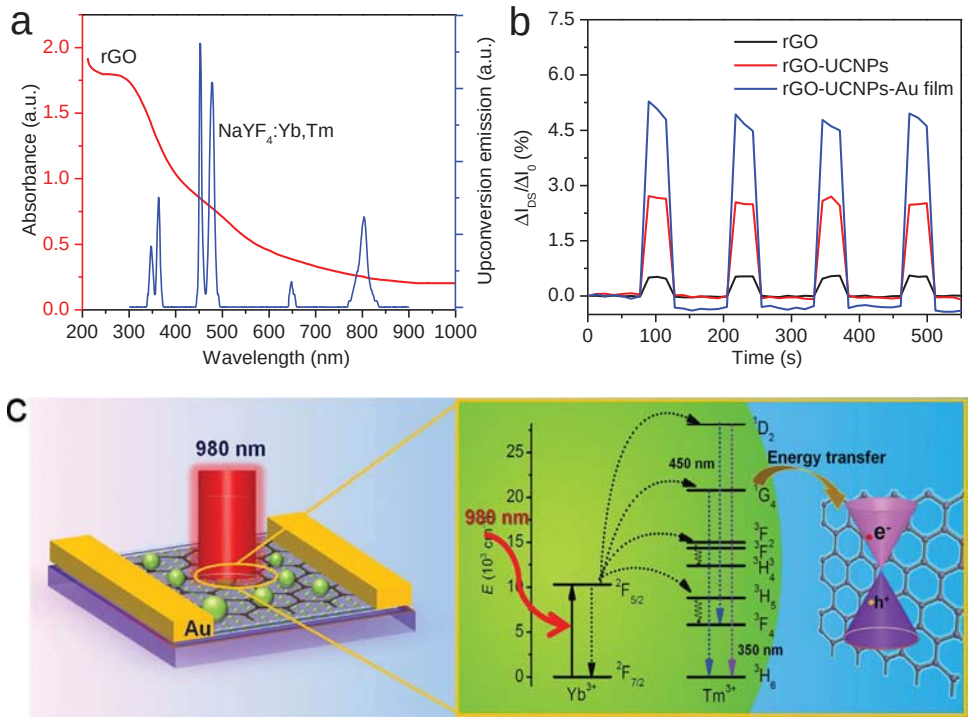

Figure 4. a) Absorption spectrum of rGO solution and upconversion emission spectrum of UCNPs, b) real-time measurements of the normalized drain current of near-infrared photoresponse devices while the 980-nm IR light is switched on and off with V_{DS} 10 mV, ΔI_{DS} represents the channel current change between the source and drain electrodes, ΔI_0 is the average minimum current response. rGO, rGO-UCNPs, and rGO-UCNPs-Au film represent the devices prepared with the layers of rGO, rGO-$NaYF_4$:Yb,Tm@$NaYF_4$ nanocomposites, and rGO-$NaYF_4$:Yb,Tm@$NaYF_4$ nanocomposites on the oxide layer-covered gold nanoparticles obtained by annealing Au film of 4 nm thickness, respectively, and c) the schematic illustration of the enhancement mechanism of near-infrared light photoresponsivity of rGO-based devices by $NaYF_4$:Yb/Tm@$NaYF_4$ UCNPs.

which provides an effectively route to improve the near-infrared photoresponse of graphene-based photodetectors. This proof-of-concept is also potential applicable in photovoltaics for improving harvesting of photons with subband-gap energies and other optoelectronic devices.[3,5a]

Experimental Section

Synthesis of $NaYF_4$:Yb,Tm Nanoparticles: For a typical synthesis, 1.0 mL of YCl_3 (0.8 mol/L), 1.0 mL of $YbCl_3$ (0.20 mol/L), 0.5 mL of $TmCl_3$ (0.01 mol/L), 6 mL oleic acid and 15 mL octadecene were added into a 100 mL flask. Then, the solution was heated to 120 °C for 10 min and to 155 °C for 30 min under stirring. After the solution cooled to 60 °C, a solution containing methanol (8 mL), NH_4F (0.148 g) and NaOH (0.10 g) was added into flask and the solution maintained for 30 min. The resulting solution was heated to 300 °C and maintained for 1.5 h under a nitrogen atmosphere. After heating was stopped, the reaction solution was cooled to room temperature and absolute ethanol was added to precipitate the fluorides UCNPs. The nanoparticles were isolated by centrifugation and redispersed in 8 mL hexane.

Synthesis of $NaYF_4$:Yb,Tm@$NaYF_4$ Core/Shell UCNPs: YCl_3 (0.8 mol/L, 1.25 mL) and oleic acid (6 mL) and octadecene (15 mL) were added to a 100 mL flask under stirring. This mixture was heated to 120 °C for 10 min and then to 155 °C for 30 min to form a clear solution before cooling to 50 °C. Shortly thereafter, a solution of 1 mmol of $NaYF_4$:Yb,Tm in 8 mL of hexane solution was added to the solution. After the removal of hexane, a solution of methanol (8 mL), NH_4F (0.148 g) and NaOH (0.10 g) was added, and the resulting mixture was stirred at 50 °C for 30 min, after which time the solution was heated to 300 °C under nitrogen for 1.5 h and then cooled to room temperature. The products were precipitated by ethanol and collected by centrifugation.

Synthesis of GO: GO sheets were prepared according to the modified Hummers' method. First, 2 g graphite flakes with the size of 3–5 mm were mixed with 12 mL of concentrated H_2SO_4 and kept at 80 °C for 4.5 h. Then, the solution was cool down to room temperature and sonicated for 1 h. The solution was diluted with 500 mL deionized water and filtered with 0.2 μm porous filter. The product was dried in vacuum desiccator to obtain pre-oxidized graphite powder. Subsequently, as-prepared graphite powder was slowly added into solution containing 120 mL concentrated H_2SO_4 and 15 g $KMnO_4$ and stirred for 2 h. The solution was diluted with 250 mL deionized water and stirred for 2 h. The mixture was further diluted with 700 mL deionized water, and then H_2O_2 (20 ml) was added to decompose the residual $KMnO_4$. The solution was kept overnight and only the upper portion of the mixture was collected and exfoliated. Then the GO was washed with diluted HCl aqueous solution and water. Finally, the GO solution was obtained after further purification by dialysis (cutoff 3000MW) against deionized water for one week.

Preparation of Ligand-Free $NaYF_4$:Yb,Tm@$NaYF_4$ Core/Shell UCNPs and GO-UCNPs Nanocomposites: The prepared oleate-capped $NaYF_4$:Yb,Tm@$NaYF_4$ UCNPs (2 mmol) was added into 15 mL HCl (0.1M) solution and ultrasonicated for 20 min. Then,

DOI: 10.1002/smll.201400400

10 mL of hexane was added into solution to abstract the stripped oleic acid ligand, and repeated at least for three times. The ligand-free $NaYF_4$:Yb,Tm@$NaYF_4$ core/shell UCNPs were obtained by centrifugation and washing with deionized water, and re-dispersed in water. For the preparation of GO-$NaYF_4$:Yb,Tm@$NaYF_4$ nanocomposites, 1.5 mL of as-prepared ligand-free UCNPs (0.15 mmol/mL) was added into 5.0 mL GO solution (0.2 mg/mL, pH 3.0). The mixture was then stirred for 10 min at room temperature to obtain GO-UCNPs nanocomposites.

Deposition of Gold Monolayer Nanoparticles with a Spacer Layer: Typically, 4 and 8 nm thick gold thin films were sputtered respectively on cleaned glass substrate, followed by a thermal annealing process at 350 °C for 15 min to form a monolayer of gold nanoparticles with the sizes of 28 and 68 nm. Then, a 8 nm amorphous TiO_2 spacer layer was deposited by home-made Atomic Layer Deposition system.

Fabrication of Devices: The solution (150 μL) of GO-$NaYF_4$:Yb,Tm@$NaYF_4$ UCNPs nanocomposites was drop-casted onto the surface of gold nanoparticles-deposited substrate (1 × 1.5 cm) with a spacer layer and dried at 50 °C. For the reduction of GO, the samples were put into glass petri dish and 500 μL of 98% hydrazine was placed in the edge of the petri dish. The petri dish was sealed and kept at 70 °C for 15 h. After that, the gold electrodes (80–100 nm thick) were evaporated on the samples through a metal mask to form a 200 μm gap where light is illuminated.

Characterization: Field-emission scanning electron microscopy micrographs were taken using a JEOL JSM-6340 instrument with 5 kV accelerating voltage. TEM images were recorded using JEOL-2010 with 200 kV accelerating voltage. The absorption spectra were measured in a spectrophotometer (Varian, Cary 5000). Upconversion spectra and lifetimes were determined at room temperature under excitation of 980 nm CW diode laser. Electrical properties were monitored with a Keithley semiconductor parameter analyser, model 4200-SCS. The power density of 980 nm laser source used for photoresponse measurements was 8 W/cm^2.

Supporting Information

Supporting Information is available from the Wiley Online Library or from the author.

[1] a) G. Konstantatos, E. H. Sargent, *Nat. Nanotechnol.* **2010**, *5*, 391; b) S. A. McDonald, G. Konstantatos, S. G. Zhang, P. W. Cyr, E. J. D. Klem, L. Levina, E. H. Sargent, *Nat. Mater.* **2005**, *4*, 138; c) G. Konstantatos, I. Howard, A. Fischer, S. Hoogland, J. Clifford, E. Klem, L. Levina, E. H. Sargent, *Nature* **2006**, *442*, 180; d) F. N. Xia, T. Mueller, Y. M. Lin, A. Valdes-Garcia, P. Avouris, *Nat. Nanotechnol.* **2009**, *4*, 839; e) A. L. Campbell, R. R. Naik, L. Sowards, M. O. Stone, *Micron* **2002**, *33*, 211.

[2] a) B. Chitara, L. S. Panchakarla, S. B. Krupanidhi, C. N. R. Rao, *Adv. Mater.* **2011**, *23*, 5419; b) J. Huang, M. Larisika, W. H. D. Fam, Q. He, M. A. Nimmo, C. Nowak, I. Y. A. Tok, *Nanoscale* **2013**, *5*, 2945; c) J. Huang, D. Fam, Q. He, H. Chen, D. Zhan, S. H. Faulkner, M. A. Nimmo, A. I. Yoong Tok, *J. Mater. Chem C* **2014**, *2*, 109; d) M. Larisika, J. Huang, A. Tok, W. Knoll, C. Nowak, *Mater. Chem. Phys.* **2012**, *136*, 304.

[3] F. J. G. de Abajo, *Science* **2013**, *339*, 917.

[4] T. Mueller, F. N. A. Xia, P. Avouris, *Nat. Photonics* **2010**, *4*, 297.

[5] a) F. Bonaccorso, Z. Sun, T. Hasan, A. C. Ferrari, *Nat. Photonics* **2010**, *4*, 611; b) Z. H. Sun, Z. K. Liu, J. H. Li, G. A. Tai, S. P. Lau, F. Yan, *Adv. Mater.* **2012**, *24*, 5878; c) H. G. Yan, X. S. Li, B. Chandra, G. Tulevski, Y. Q. Wu, M. Freitag, W. J. Zhu, P. Avouris, F. N. Xia, *Nat. Nanotechnol.* **2012**, *7*, 330.

[6] G. Konstantatos, M. Badioli, L. Gaudreau, J. Osmond, M. Bernechea, F. P. G. de Arquer, F. Gatti, F. H. L. Koppens, *Nat. Nanotechnol.* **2012**, *7*, 363.

[7] a) P. Hazarika, D. A. Russell, *Angew. Chem. Int. Ed.* **2012**, *51*, 3524; b) B. P. Jackson, D. Bugge, J. F. Ranville, C. Y. Chen, *Environ. Sci. Technol.* **2012**, *46*, 5550; c) X. J. Xie, N. Y. Gao, R. R. Deng, Q. Sun, Q. H. Xu, X. G. Liu, *J. Am. Chem. Soc.* **2013**, *135*, 12608; d) S. W. Wu, G. Han, D. J. Milliron, S. Aloni, V. Altoe, D. V. Talapin, B. E. Cohen, P. J. Schuck, *Proc. Natl. Acad. Sci. U.S.A.* **2009**, *106*, 10917.

[8] a) F. Wang, R. R. Deng, J. Wang, Q. X. Wang, Y. Han, H. M. Zhu, X. Y. Chen, X. G. Liu, *Nat. Mater.* **2011**, *10*, 968; b) J. Wang, F. Wang, C. Wang, Z. Liu, X. G. Liu, *Angew. Chem. Int. Edit.* **2011**, *50*, 10369; c) L. Cheng, K. Yang, Y. G. Li, J. H. Chen, C. Wang, M. W. Shao, S. T. Lee, Z. Liu, *Angew. Chem. Int. Ed.* **2011**, *50*, 7385; d) G. Tian, Z. J. Gu, L. J. Zhou, W. Y. Yin, X. X. Liu, L. Yan, S. Jin, W. L. Ren, G. M. Xing, S. J. Li, Y. L. Zhao, *Adv. Mater.* **2012**, *24*, 1226; e) J. L. Liu, Y. Liu, Q. Liu, C. Y. Li, L. N. Sun, F. Y. Li, *J. Am. Chem. Soc.* **2011**, *133*, 15276; f) A. Bednarkiewicz, M. Nyk, M. Samoc, W. Strek, *J. Phys. Chem. C* **2010**, *114*, 17535; g) L. J. Charbonnière, N. Hildebrandt, R. F. Ziessel, H. G. Löhmannsröben, *J. Am. Chem. Soc.* **2006**, *128*, 12800; h) L. J. Charbonnière, N. Hildebrandt, *Eur. J. Inorg. Chem.* **2008**, *21*, 3241.

[9] a) N. J. J. Johnson, A. Korinek, C. H. Dong, F. C. J. M. van Veggel, *J. Am. Chem. Soc.* **2012**, *134*, 11068; b) F. Wang, L. D. Sun, J. Gu, Y. F. Wang, W. Feng, Y. Yang, J. F. Wang, C. H. Yan, *Angew. Chem. Int. Ed.* **2012**, *51*, 8796; c) Y. Liu, M. Chen, T. Y. Cao, Y. Sun, C. Y. Li, Q. Liu, T. S. Yang, L. M. Yao, W. Feng, F. Y. Li, *J. Am. Chem. Soc.* **2013**, *135*, 9869; d) Q. Q. Su, S. Y. Han, X. J. Xie, H. M. Zhu, H. Y. Chen, C. K. Chen, R. S. Liu, X. Y. Chen, F. Wang, X. G. Liu, *J. Am. Chem. Soc* **2012**, *134*, 20849; e) F. Wang, Y. Han, C. S. Lim, Y. H. Lu, J. Wang, J. Xu, H. Y. Chen, C. Zhang, M. H. Hong, X. G. Liu, *Nature* **2010**, *463*, 1061; f) F. Wang, X. G. Liu, *Chem. Soc. Rev.* **2009**, *38*, 976; g) F. Wang, X. G. Liu, *J. Am. Chem. Soc.* **2008**, *130*, 5642; h) Z. Q. Li, Y. Zhang, S. Jiang, *Adv. Mater.* **2008**, *20*, 4765; i) F. Zhang, Y. Wan, T. Yu, F. Q. Zhang, Y. F. Shi, S. H. Xie, Y. G. Li, L. Xu, B. Tu, D. Y. Zhao, *Angew. Chem. Int. Ed.* **2007**, *46*, 7976; j) S. Heer, K. Kompe, H. U. Gudel, M. Haase, *Adv. Mater.* **2004**, *16*, 2102; k) L. Cheng, C. Wang, X. X. Ma, Q. L. Wang, Y. Cheng, H. Wang, Y. G. Li, Z. Liu, *Adv. Funct. Mater.* **2013**, *23*, 272.

[10] E. Morales-Narvaez, A. Merkoci, *Adv. Mater.* **2012**, *24*, 3298.

[11] a) Z. Y. Hou, C. X. Li, P. A. Ma, G. G. Li, Z. Y. Cheng, C. Peng, D. M. Yang, P. P. Yang, J. Lin, *Adv. Funct. Mater.* **2011**, *21*, 2356; b) Z. Y. Hou, C. X. Li, P. A. Ma, Z. Y. Cheng, X. J. Li, X. Zhang, Y. L. Dai, D. M. Yang, H. Z. Lian, J. Lin, *Adv. Funct. Mater.* **2012**, *22*, 2713; c) J. V. Garcia, J. P. Yang, D. K. Shen, C. Yao, X. M. Li, R. Wang, G. D. Stucky, D. Y. Zhao, P. C. Ford, F. Zhang, *Small* **2012**, *8*, 3800.

[12] L. T. Su, S. K. Karuturi, J. S. Luo, L. J. Liu, X. F. Liu, J. Guo, T. C. Sum, R. R. Deng, H. J. Fan, X. G. Liu, A. I. Y. Tok, *Adv. Mater.* **2013**, *25*, 1603.

[13] a) W. Wei, T. C. He, X. Teng, S. X. Wu, L. Ma, H. Zhang, J. Ma, Y. H. Yang, H. Y. Chen, Y. Han, H. D. Sun, L. Huang, *Small* **2012**, *8*, 2271; b) T. C. He, W. Wei, L. Ma, R. Chen, S. X. Wu, H. Zhang, Y. H. Yang, J. Ma, L. Huang, G. G. Gurzadyan, H. D. Sun, *Small* **2012**, *8*, 2163; c) R. Chen, V. D. Ta, F. Xiao, Q. Y. Zhang, H. D. Sun, *Small* **2013**, *9*, 1052; d) E. M. Chan, G. Han, J. D. Goldberg, D. J. Gargas, A. D. Ostrowski, P. J. Schuck, B. E. Cohen,

small 2014,
DOI: 10.1002/smll.201400400

D. J. Milliron, *Nano. Lett.* **2012**, *12*, 3839; e) C. L. Zhang, Y. X. Yuan, S. M. Zhang, Y. H. Wang, Z. H. Liu, *Angew. Chem. Int. Ed.* **2011**, *50*, 6851; f) X. Huang, X. Y. Qi, F. Boey, H. Zhang, *Chem. Soc. Rev.* **2012**, *41*, 666; g) W. B. Niu, S. L. Wu, S. F. Zhang, L. T. Su, A. I. Y. Tok, *Nanoscale* **2013**, *5*, 8164; h) F. Wang, D. Banerjee, Y. S. Liu, X. Y. Chen, X. G. Liu, *Analyst* **2010**, *135*, 1839.

[14] a) S. Schietinger, T. Aichele, H. Q. Wang, T. Nann, O. Benson, *Nano. Lett.* **2010**, *10*, 134; b) N. Liu, W. P. Qin, G. S. Qin, T. Jiang, D. Zhao, *Chem. Commun.* **2011**, *47*, 7671.

[15] a) M. Saboktakin, X. C. Ye, S. J. Oh, S. H. Hong, A. T. Fafarman, U. K. Chettiar, N. Engheta, C. B. Murray, C. R. Kagan, *Acs Nano* **2012**, *6*, 8758; b) P. Y. Yuan, Y. H. Lee, M. K. Gnanasammandhan, Z. P. Guan, Y. Zhang, Q. H. Xu, *Nanoscale* **2012**, *4*, 5132.

[16] a) Y. Liu, R. Cheng, L. Liao, H. L. Zhou, J. W. Bai, G. Liu, L. X. Liu, Y. Huang, X. F. Duan, *Nat. Commun.* **2011**, *2*, 579; b) T. J. Echtermeyer, L. Britnell, P. K. Jasnos, A. Lombardo, R. V. Gorbachev, A. N. Grigorenko, A. K. Geim, A. C. Ferrari, K. S. Novoselov, *Nat. Commun.* **2011**, *2*, 458.

[17] N. Bogdan, F. Vetrone, G. A. Ozin, J. A. Capobianco, *Nano. Lett.* **2011**, *11*, 835.

[18] a) W. B. Niu, S. L. Wu, S. F. Zhang, *J. Mater. Chem.* **2011**, *21*, 10894; b) W. B. Niu, S. L. Wu, S. F. Zhang, *J. Mater. Chem.* **2010**, *20*, 9113; c) J. C. Boyer, F. Vetrone, L. A. Cuccia, J. A. Capobianco, *J. Am. Chem. Soc.* **2006**, *128*, 7444; d) J. C. Boyer, L. A. Cuccia, J. A. Capobianco, *Nano. Lett.* **2007**, *7*, 847; e) J. C. Boyer, J. Gagnon, L. A. Cuccia, J. A. Capobianco, *Chem. Mater.* **2007**, *19*, 3358; f) F. Vetrone, R. Naccache, A. J. de la Fuente, F. Sanz-Rodriguez, A. Blazquez-Castro, E. M. Rodriguez, D. Jaque, J. G. Sole, J. A. Capobianco, *Nanoscale* **2010**, *2*, 495.

[19] E. W. Peng, E. S. G. Choo, P. Chandrasekharan, C. T. Yang, J. Ding, K. H. Chuang, J. M. Xue, *Small* **2012**, *8*, 3620.

[20] O. Akhavan, E. Ghaderi, H. Emamy, *J. Mater. Chem.* **2012**, *22*, 20626.

[21] W. H. He, L. H. Lu, *Adv. Funct. Mater.* **2012**, *22*, 2542.

[22] S. D'Agostino, F. Della Sala, *ACS Nano* **2010**, *4*, 4117.

[23] a) W. B. Niu, S. L. Wu, S. F. Zhang, J. Li, L. A. Li, *Dalton. T.* **2011**, *40*, 3305; b) F. Vetrone, V. Mahalingam, J. A. Capobianco, *Chem. Mater.* **2009**, *21*, 1847; c) F. Vetrone, R. Naccache, V. Mahalingam, C. G. Morgan, J. A. Capobianco, *Adv. Funct. Mater.* **2009**, *19*, 2924.

Received: February 13, 2014
Revised: April 17, 2014
Published online: